

SURFACE VISUALISATION OF TIME AVERAGED FLOW BEHAVIOUR AROUND RIGID AND FLEXIBLE HEMISPHERES UTILISING UV SENSITIVE OIL

Nishanth Menakath¹, Nicholas J. Lawson¹ & Gareth A. Vio²

¹School of Aerospace, Mechanical and Mechatronic Engineering, The University of Sydney, NSW 2006, Australia ²Defence Science and Technology Group, Port Melbourne, Melbourne 3201 VIC, Australia

Abstract

Experimental testing has been conducted to provide a comparison between the surface flow characteristics around a thin walled, flexible hemisphere and a rigid hemisphere (D = 100mm) immersed within a turbulent boundary layer, to observe the variance due to fluid-structure interactions. A comparison of the effects of a thin flexible membrane on the flow features, both downstream and within the immediate surrounding region, have been observed using oil flow visualisation. While used as a qualitative method of analysis, the flow visualisation has been coupled with edge detection methods. This has allowed extraction of the time averaged effects of a flexible bluff body in comparison to a rigid bluff body. Specifically, including the growth of the wake region, the size, and shape of surface flow features and the effects of incoming flow speed on the flow features surrounding the models. Testing has been conducted through a flow velocity range of 15m/s to 40m/s. Results have indicated a change in the wake of the flexible structure, in comparison to the rigid structure. In this case, the flexible model wake shows larger growth at low speeds, with a consistently higher rate of wake growth comparative to the rigid model. This effect, however, is minimised as the flow velocity is increased, showing that at 40m/s, wake growth aft of the flexible and rigid structure appear similar. The absolute magnitude remains similar between the flexible and rigid model, being y/D = 1.675 and y/D = 1.76 respectively at 2.5D downstream. The rate of wake growth is largest at low speeds, with the flexible model showing 68% spanwise increase compared with 25% increase for the rigid model. A spanwise asymmetry has also been observed in the flow pattern, as the flexible model shows larger wake spanwise asymmetry farther from the model. Compared with the rigid model, the wake asymmetry at 2.5D downstream was measured as y/D = 0.47 for the flexible hemisphere, whilst being $y/D \approx 0$ for the rigid model, both at 40m/s. Edge detection techniques, applied to time averaged oil flow visualisation, further identified that for flow with regions of high contrast, the method can be utilised to capture the wake criteria.

Keywords: Oil based Flow visualisation, Flow-visualisation, Fluid-Structure Interaction, Boundary layer flow, Image Processing Techniques

1. Introduction

Investigations of the fluid structure interaction of small-scale protuberances immersed within a turbulent boundary layer, has been conducted with the aim of understanding of flow features around such structures. The primary application is the implementation of protuberances as sensor shrouds for externally mounted components. For this analysis, the protuberance model is a hemisphere, to act as a simplified representation of an externally mounted shroud. Previous research has presented investigations of the flow structures around rigid hemispherical structures. However, to further extend this line of research, the comparison between deformable/flexible structures is investigated. The technique employed for the comparisons is oil visualisation. This technique is extensively used to provide qualitative analysis of flow patterns and flow behaviour for numerous aerospace and fluid analysis applications. Papers including Lu (2010)[1] and Koklu (2018)[2] have shown the application of qualitative analysis of the flow characteristics have been used in conjunction with numerical

modelling, to gather quantitative data. To enable comparison of the flow behaviour around a rigid hemisphere and flexible hemisphere, oil visualisation and edge detection, have been used to gather both quantitative and qualitative insight. The utilisation of image processing techniques allows rapid and consistent analysis of flow features, for experimental flow visualisation techniques.

1.1 General Flow Features

Flow features around rigid hemispheres is an area of research that has been investigated over several decades. This paper has extended this research through observation of large-scale surface flow characteristics around both rigid and flexible hemispheres. Ultraviolet (UV) oil based visualisation and edge detection/image processing techniques have been used to record and present quantitative data, from oil visualisation. This technique has historically been used for qualitative analysis of the wake formation and flow separation. Of interest in this work, is the effect a flexible membrane has on the large flow structures in the wake and the aeroelastic interaction, between the deformation of a flexible structure and the surrounding flow.

With the flow around a hemisphere, specifically in the wake, the dominant flow characteristic is the shedding of vortex structures, specifically (vK) von Kármán vortices from the body, as described by Savory & Toy (1986).[3] This previous work clearly identified that the boundary layer formation has a substantial effect on the formation of the wake structures around the hemisphere structure. Experiments by Savory & Toy (1986)[3] were conducted at a lower Reynolds number than the current testing. For a direct comparison to the current experiment, McCarthy et al. (2018)[4] presented comparative data for the flow behaviour around a rigid hemisphere. This data looked at the wavelet coherence of the surface pressure fluctuation in the near wake region of a rigid hemisphere. The Reynolds number in this case was $Re_D = 6.36 \times 10^4$. Like the testing completed within this paper, surface visualisation is achieved using china-clay; allowing for clear visualisation of the formation and development of the vortex structures within the wake region. Here, time-averaged data is presented through qualitative images to characterise the general wake formation and vortex structures. Manhart (1998)[5] further elaborates on the work conducted by Savory & Toy (1986)[3], through use of a Large Eddy Simulation (LES) of the vortex shedding around a hemisphere at Re = 150,000. Being comparable to the testing conducted here, the primary findings of Manhart (1998)[5] confirms the observations made previously by existing work. Specifically, the identification of two key driving mechanisms for the near-wake region. That being the separation and roll-up of the shear layer at the top of the hemisphere and the separation of the vK vortex structures from the side regions of the hemisphere. However, all behaviour described is primarily attributed to periodic or quasi-periodic behaviour. Specifically, the two mechanisms driving the behaviour, are identified to have Strouhal numbers of 0.5 and 0.2 respectively. This behaviour will be time-averaged for this work, thus not able to resolve the effects of periodic changes in the wake structure. From this work, the key observations made regarding the flow structures are also identified in previous work conducted by Menakath et al. (2023).[6] Where the evaluation of pressure fluctuations around the rigid hemisphere is utilised to gather an understanding of the general flow structure in the surrounding wake which better allows for analysis of temporal effects in the flow.

Carr & Plesniak (2015)[7] have also observed the flow around a hemisphere in a pulsatile flow. They found that in typical, positive inflow conditions, the recirculation arch (RA) vortex structure trends reliably downstream, collapsing into the aft wake structure. In the pulsatile flow tested, they noted that this behaviour dissipates further upstream and towards the wall of the tunnel. As the flow conditions for the current testing procedure have typical positive inflow conditions, it can be expected that the former behaviour will be found in this work. Wood et al. (2020)[8] has previously shown a comparison between the aero-elastic interactions between both a thin walled membrane and a rigid structure and the surrounding flow. This work is primarily focused on the flow effects upon structural surface distortions, with a generalised exploration of the vortex structure formation and dissipation. Specifically, the structure used during the testing is an air-inflated hemisphere, held at a constant pressure during the testing procedure. Wood et al. (2020)[8] identifies that the largest deflection of the flexible model occurs at the forward facing top region of the hemisphere, from 80% to 100% of the vertical distance, as expected during this experiment as well. Wood et al. (2020)[8] furthermore evaluates the side profile of the time averaged flow field, when comparing the flexible and rigid structure. The

key finding noted that at Re = 75,000, the flexible hemisphere caused the formation of an elongated "belly shaped" recirculation region, due to the movement of the detachment line on the surface of the flexible model. This caused by the morphing of the structure from the variance of oncoming flow conditions. The work presented in this paper will expand the data of the previous papers.

1.2 Oil Flow Visualisation

Flow visualisation, particularly, oil visualisation has been an effective tool utilised primarily for qualitative visualisation of flow features and behaviour. The medium of oil flow visualisation primarily uses oil as a carrier medium, to transport reflective particles, enabling deposition of the particles across a surface dependent on the local flow pattern in the region. The early foundations of this technique are described by Maltby (1962) where, with exhaustive detail, explains the process of oil visualisation. Numerous methods are provided as techniques to use, of particular importance is the use of china clay and kerosene. For this paper, the primary oil used is paraffin oil which in practice is comparable to the kerosene used by Maltby (1962).[9] In addition, when considering additives to the oil mixture; oleic acid is used by Maltby (1962) for a mixture to titanium dioxide-kerosene paint. This additive is specified to enable the particulates to disperse within the oil mixture at low quantities (<10%) with the oleic acid, further resulting in clear "streaks" forming showing the deposition of the titanium dioxide particles throughout the test structure. Without the addition of the oleic acid, only regions of high shear were clearly visible.[9]. For this experimental procedure, a modification in the oleic acid ratio is used coupled with a replacement of the titanium dioxide pigment to that of cornstarch pigment, due to availability. The exact mixture used for testing is specified in section 2.1. Another example of similar oil flow utilisation is presented in Hunt et al. (1978)[10] which presents the distribution of flow around a cuboid using "Crisco oil" as the medium with zinc oxide powder as the pigment. The results show exceptional detail in the freestream and upstream region; however, the mixture lacks the ability to clearly resolve the near wake structure. The far wake is resolved when the bluff body is perpendicular to the flow, however once rotated to 47° the far wake has a lower level of contrast. This could be attributed to the mixture clearly capturing the high shear regions, but possessing lower capability to resolve lower shear regions.[10] Due to the similarity between the test shape used for this paper, similar bulk flow features are visible. The features are reiterated with a comparative study presented by Merzkirch (1987)[11], in which he takes note of the skin friction of the oil and the comparative viscosity ratio between the oil and the air. Particularly noting the inadequacy of measuring the exact location of flow separation with oil visualisation exclusively. This is of note for the testing conducted in this paper.

Described experimentally by Wood et al. (2018) [8] and computationally Cao and Tamura (2020) [12] the point at which flow separation occurs will directly impact the behaviour of the rear wake and thus is not completely captured by the oil visualisation technique used here. However, the oil lines on the surface of the hemisphere for this test can be an indication of inherent 3-dimensional flow the models experience. With true characterisation of the 3-dimensional separation and reattachment downstream requiring further research. This point of 3-dimensional flow separation has been discussed by Tobak and Peake (1982) [13] however for the purpose of this experimentation, this region of analysis is of less importance comparative to the flow in the surrounding surface plane. Further analysis of flow separation and the resulting surface flow topology has been characterised by Simons and Corke (2019) [14] and Koklu (2018) [2], though both papers looked at the oil flow visualisation on flat curved surfaces, the regions identified show similarity to the expected flow patterns observable in this experiment. The key aspects of both papers are the identification of focus and saddle points and the relation to the flow separation. Particularly of observation is the detachment line visualisation presented by Koklu (2018) [2], though different in root cause for this paper, the pattern presented by the past research is somewhat replicated from the conducted testing, indicating that the pattern observed in the current work is analogous to previously described flow patterns. For this instance, the detachment lines pertain directly to the shed vortices along the spanwise sides of the hemisphere structure. Thus, the use of oil flow visualisation is a well-known and utilised technique, coupling this with quantification through edge detection allows for data pertaining to specific flow pattern and flow behaviour to be extracted from the typically qualitative flow visualisation.

1.3 Edge Detection Method

Edge detection methods are a well-used piece of computational post-processing applied to images to enable the extraction of pixel data pertaining to the boundary of objects within a given image. The Canny algorithm is a popular and advanced method utilised for this purpose and is the basis of the analysis conducted for this paper. The Canny algorithm, first developed and presented in Canny (1986) allows for pixel intensity gradient evaluation to detect the edges of a given image.[15] The basic algorithm is operated by applying a low-pass Gaussian filter across the image. The image intensity gradient is obtained to evaluate the regions with larger magnitude spatial derivatives. The edge detection method tracks the gradient peaks along the domain, storing them as a binarised output. The output is always shown as normal to the gradient direction. All pixels not located on the detected edge are removed using a non-maximum suppression method. The final operation of the Canny filter is to apply a threshold bound, which limits the minimum and maximum threshold for the intensity gradients. This allows for the manipulation of the algorithm controlling the gradient magnitude desired for an edge to be validated as a "real" edge or omitted as noise or an invalid edge.[16] This methodology is utilised within this analysis for final data extraction.

Edge detection methods have been utilised in the observation of flow behaviour in past literature. Znamenskaya et al. (2020) utilised the Canny edge detection method, among others, to enable the extraction of edges from Schlieren and shadowgraph images.[16] The main purpose of the research was to compare the effectiveness of using a Canny edge detection compared with a Neural network. When directly observing the Canny effectiveness, it was identified for the three distinct flow structures, the Canny method was effective at resolving the edges of shock waves, quiescent air and convective streams. The work concluded that the Canny method can be effectively used as a baseline for further implementation of edge detection algorithms due to the accuracy of prediction of flow features. Fujimoto et al. (2019) also shows the utilisation of a Canny edge detection, modified with the use of Rankine-Hugonoit conditions to evaluate shocks.[17] The method utilised shows considerable reduction in computational time required to process images to resolve the edges of the shock patterns. The method indicates that when observing cases with oblique shocks, the method can detect both the primary shocks along with the reflected shock, with no false edge detections. The research does indicate that the method can detect edges in both numerical inviscid flow cases and viscous flow. Abdelsalam et al. (2017) directly utilise tracking of oil flow pattern edges using the Canny filter as a technique to compare flow feature spatial locations with that of computational results.[18] The edge detection algorithm, utilising the Canny operator as a basis, presents accurate results indicates the similarity with physical measurements of the saddle point with <0.5 mm variance, which was estimated as within the measurement precision of the physical ruler. Generally, this work indicates and recommends that the extraction of quantitative data from surface flow visualisation can be accomplished with accuracy using standard image processing techniques such as Canny edge detection. Limitations do exist with the Canny method however, as noted by Guo et al. (2010), where they noted the tendency of the Canny method to have difficulty with distinguishing the edges of small scale flow structures especially when there is strong noise in the signal and substantial levels of light reflection.[19] This issue is minimised by the processing of the images, as shown within this paper.

2. Experimental setup

The experiment was conducted within the University of Sydney 3ft by 4ft closed loop wind tunnel. Figure 1 presents a diagram of the testing setup used for experimentation. Both the flexible and rigid models were mounted to a tunnel mid-plane with a 2:1 elliptical leading edge, allowing for a turbulent boundary layer to develop. The mid-plane was positioned to eliminate wall effects from the wind tunnel itself. During previous testing of the wind tunnel, between the velocity ranges of 10m/s to 25m/s, the turbulence intensity was measured as 0.15% to 0.2%, with an expected decrease in turbulence intensity with increasing test velocity. The test section was placed 4.9D downstream of the leading edge of the mid-plane with a black acrylic mid-plane insert to allow for maximum contrast with the UV sensitive liquid.

In figure 1, UV sensitive liquid was distributed in a thin layer around and on the model itself such that uniform coverage of the region of interest was obtained. The primary region of interest is the

black acrylic mid-plane insert. A digital single-lens mirror-less (DSLM) camera was positioned above the test setup, exterior to the wind tunnel, mounted on a traverse system. The camera was also positioned parallel to freestream, with the lens parallel to the mid-plane. As all readings were taken as time-averaged results; the wind tunnel operated for 10 minutes to allow for sufficient deposition of the particulates within the visualisation mixture. The wind tunnel operated at the specified test velocities ranging from 15m/s to 40m/s, providing time for the oil to distribute along the surface of the mid-plane. Allowing for sufficient time to enable the paraffin oil to dry, minimising pooling of fluid. Following this, two 50W UV emitting LED light arrays were positioned upstream and downstream of the test section and a series of images of the oil distribution were taken. This process was then repeated for each subsequent velocity case and for each model. This testing procedure allowed for the extraction of time averaged results. Testing was conducted over the course of multiple days with varying environmental conditions, as a general overview of testing conditions, the flow regime from 15m/s to 40m/s corresponds to $Re \approx 90,000$ to $Re \approx 250,000$.

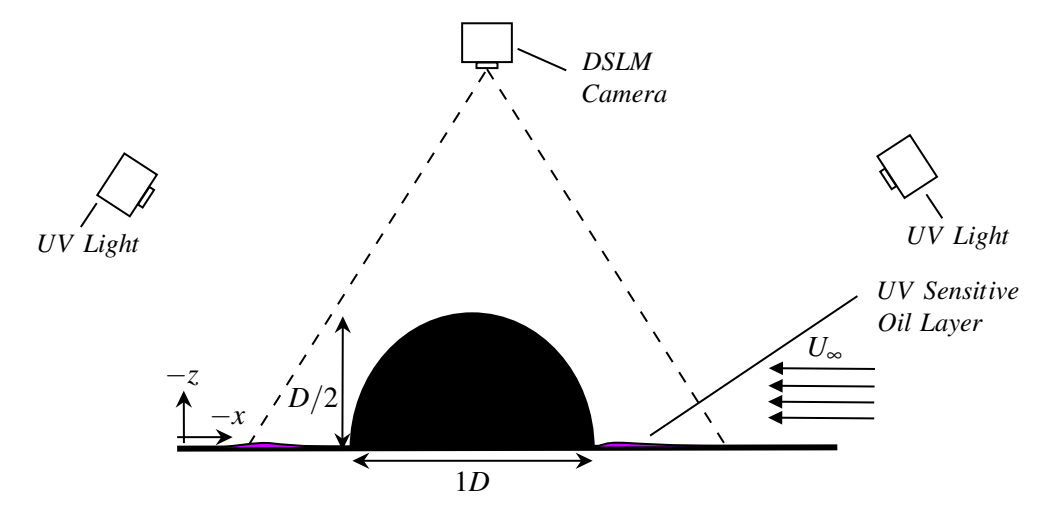


Figure 1 – Diagram of Test Setup

2.1 Oil Mixture

The oil base utilised is paraffin oil as the medium for deposition of smaller particulates of cornstarch powder. Allowing the wind tunnel to run for a minimum of 5 minutes per test run allows for the oil to be shifted downstream and dried, leaving behind the cornstarch mixture dyed with RC-77 Dye Penetrant, highlighting the flow features. However, for lower velocity cases, a longer test time is utilised to allow for the oil to adequately dry. The flow visualisation mixture consists of; 85g of Cornstarch Powder, 250ml of Paraffin oil, 5ml of oleic acid and 4ml RC-77 Fluorescent Dye Penetrant. The mixture ratios are maintained, with variance in the quantity created per batch. The general process to form the usable mixture begins with the combination of the cornstarch power and paraffin oil. This blend is mixed thoroughly such that the powder is distributed within the paraffin oil equally. Following this, the oleic acid and fluorescent dye are combined into the solution and mixed until the resulting liquid is observably homogeneous. The primary purpose of the oleic acid being that of an emulsifying agent, acting similarly to the mixture described in Maltby (1962)[9]. The liquid mixture is then painted onto the testing surface with a paintbrush, providing even coverage around all models and the region of interest.

2.2 Test Models

For the experiment, two models were created; a flexible thin walled membrane and a rigid hemisphere. The diameter of both models were, D=100mm with connection of the rigid model to the mid-plane provided using a singular M6 bolt, allowing for a flush connection to be created between the structure and the mid-plane. The flexible model uses a 3d printed mounting plate which forces the structure to adhere to the mid-plane with the use of 4 M6 bolts. The rigid model has been constructed using 3D printed PLA (Polylactic acid) plastic. To achieve the desired surface finish, the surface of the

rigid article has been sanded and smoothed down with 1000 grit sandpaper and gap-filler used where required. For the creation of the flexible structure, polyurethane resin, with a Shore A-15 hardness rating, was used to cast a thin shelled membrane with a 3.5mm wall thickness. Figure 2 presents an image of the rigid model used in testing. Figure 3 shows the flexible model used in testing, whilst Figure 4 shows a qualitative example of the static deformation of the flexible hemisphere with a 1kg weight applied at the hemisphere apex.







Figure 2 – Rigid hemisphere model

Figure 3 – Flexible hemisphere model

Figure 4 – Deformation of flexible hemisphere

3. Results

Testing was conducted with a rigid model and a flexible model at flow velocities ranging from 15m/s to 40m/s. Edge detection methods subsequently calculated the change in flow features, due to model and Reynolds number variance. During testing, images were taken at a range of exposure levels to gather a large set of contrast levels for the final processing. To process the data, initially the images are imported from a high-resolution '.jpg' format to MATLAB, enabling the image to be converted from an RBG format to a grayscale image. Due to the nature of particle deposition across the mid-plane, there is an elevated level of noise within the grayscale image, preventing the extraction of distinct and clearly observable edges. Thus, prior to the edge detection being utilised, a filtering process was applied to enable the higher frequency components of a spatial fast-Fourier transform to be removed, giving higher quality edge detection, less prone to false detection or omissions.

3.1 Qualitative comparison of flow features

Figure 7 and figure 8 present an example of the qualitative visualisation of the time average flow patterns around the both models at 40m/s whilst Figure 5 and figure 6 present a qualitative visualisation of the time average flow patterns around the both models at 15m/s. All images have been zoomed into the near-structure region for clarity. The downstream flow region shows some variance in behaviour, as expected, with both a change in the model and a change in the flow speed. When considering the effect of flow speed variation between figure 5 and figure 7 or figure 6 and figure 8, commonalities can be observed which are consistently evident between models at the minimum and maximum test velocities. The primary observation that can be made is the growth of the wake size. With the increase in flow velocity, there is a noticeable increase in the size of the downstream wake, particularly the angle at which the wake boundary interacts with the surrounding freestream. This increase in wake size is far more apparent when observing the rigid model. The flexible model does not show a substantial size difference at the far downstream position, however the rate of growth and the starting size of the wake region increases within velocity. Between the boundary of the wake and the freestream flow, the hairpin vortex structure as described by McCarthy et al.(2018) [4] is observable as originating at the port and starboard side of both the flexible and the rigid hemisphere models. The vortex structure can be observed to trap a substantial amount of oil within, causing a distinct boundary to form between the wake and the freestream. This feature is the critical flow feature analysed using the method described in this paper, due to the clearly defined illumination gradient between this flow feature and the surrounding regions.

Aft of the main model itself, a localised region of flow circulation can be observed. This recirculation region causes pooling of the oil mixture in this region, proportional to the size and strength of the recirculation. As the velocity is increased, the size of this region diminishes, with the figure 8 showing that for the flexible model, the recirculation region is completely absent. For the 15m/s cases, the instability of the flow caused by the flexible model further causes the recirculation region to deform into a random, fractal-like pattern whilst the rigid model recirculation remains as two circular structures. In the far wake region, the primary difference between the low speed and high speed test cases are the flow instabilities. This behaviour is more pronounced at lower velocities, appearing as localised regions of oil particle deposition in the freestream region of the aft flow. At lower velocities, the flow instability obfuscates the exact boundary of the wake, this necessitates some interpretation of the wake edge during analysis. This feature also shows that the hairpin vortex structure collapses into the freestream and wake at a point further upstream for the flexible model as compared to the rigid model. The amount of these structures is lessened for the rigid model, however the behaviour is still present, indicated by the regions of high oil retention in the wake, as seen in figure 5. In figure 6 the level of flow instability is at a higher level with large regions of oil deposition persisting. This can be directly attributed to the effect of the fluid-structure interaction, however as this result is time averaged, only inferences can be made for the root cause of the behaviour. As the velocity is increased to 40m/s the flow instability for the flexible model persist however the magnitude is reduced substantially, as indicated by the size of the oil droplets in the aft region as shown in figure 8. This is not observable for the rigid model shown in figure 7.

Another difference for higher speed cases is the variation in the internal wake structure, with the reat-tachment point of the flow aft of the flexible model showing a larger spanwise growth, as compared to the rigid model. This causes an apparent difference in the two main wake sub-regions. The first region is the inner region, originating from the aft side of the structure and the direct interaction of the reattached flow from the structure itself. The second region is the outer wake region, which originates along the port and starboard side of the structure, which in turn originates at the leading edge of the model. The boundary of the outer wake region can be observed to extend to the upstream face of the model, with the size of the region shown as larger for the rigid model as compared to the flexible model. At 40m/s, the reattachment point of the shear layer aft of the rigid structure, shows a smaller region of reattachment, whilst the flexible model shows the reattachment region directly effecting the wake formation. Some features of this behaviour have been extracted using the edge detection method to validate the qualitative observations made.

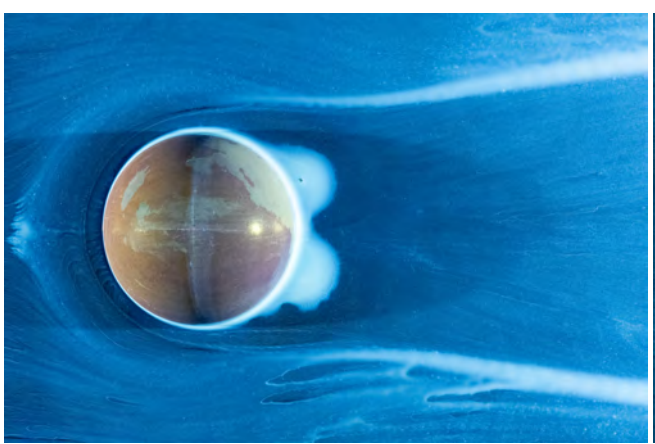


Figure 5 – Flow at 15m/s Surrounding Rigid Hemisphere



Figure 6 – Flow at 15m/s Surrounding Flexible Hemisphere

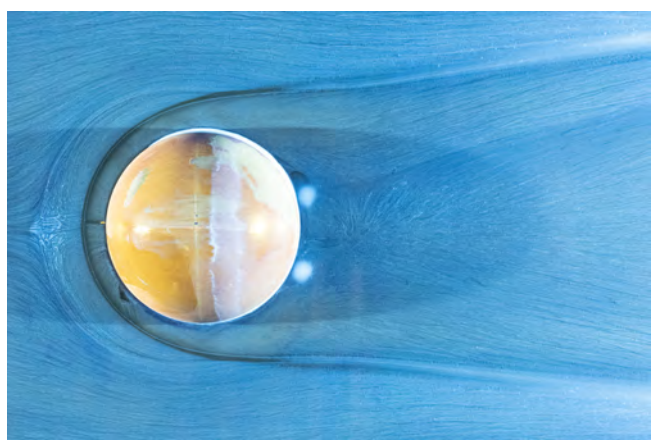




Figure 7 – Flow at 40m/s Surrounding Rigid Hemisphere

Figure 8 – Flow at 40m/s Surrounding Flexible Hemisphere

Zooming into the leading edge allows for greater clarity in the images presented. What can be noted here is the prominence of the interface between the freestream flow and the flow immediately on the surface of the hemisphere itself. When observing the flow around the leading edge shown in figure 5, 6, 7 and 8, the observation that can be made is the similarity between the leading edge behaviour between the two velocity cases shown. Thus, to demonstrate an example of the flow behaviour in detail, figure 9 and figure 10 shows a zoomed-in leading edge for the 40m/s case to demonstrate an idealised viewing window of the dataset. For the rigid structure, the surrounding region appears uniform without variation when analysing the complete circumference of the hemisphere. Figure 9 presents a smaller region of flow disturbance surrounding the rigid structure, with more variance between the starboard and port side of the hemisphere surface. This region, as specified in section 3.1 travels downstream into the wake and comprises a component of the outer wake region. The region immediately surrounding the model itself is larger in radius for the rigid model as compared to the flexible (figure 10), with more spanwise deflection at the port and starboard side of the flexible model. This can be linked to the variation in wake size observed previously. The leading edge structure size remains consistent between the flexible and the rigid model. The region of flow redirection at the leading edge, travelling further upstream for the rigid model also shows a minor variation in the spanwise dimension.



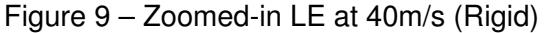




Figure 10 – Zoomed-in LE at 40m/s (Flexible)

The qualitative analysis allows for a simple understanding of the major components of the flow structure to be identified. This allows for the subsequent processing of the acquired images to extract flow parameters and compare the flow surrounding the two models.

3.2 Edge Detection Method

The method of edge detection used within this paper is the Canny method (1986) [15]. The images shown in section 3.1 indicates the nature of particle deposition in the domain of interest. Directly using these images within the Canny algorithm will generate a large degree of false edges, inconsistent with the flow behaviour. The major aspects that will be compared using the edge detection implementation is the wake size, particularly the relative growth of the wake when comparing the rigid and flexible hemisphere at 15m/s to 40m/s. A general example of the post-processing process is provided within this section.

The initial stage in processing the input images is the conversion of the RGB image to a grayscale, to allow for the detection of brightness fluctuations ranging from integer value 0 to 255. However, the resulting image contains a high level of noise, as visible in figure 11. An initial array of cross-sectional data points are taken at the line locations shown in figure 11. The acquired datasets are utilised as the baseline to evaluate the number of expected streamlines in the regions of interest, allowing for windowing of the solution to remove noise. The upstream Y-axis line is utilised to gather an input of freestream streamline quantity, whilst the downstream is utilised as a comparative tool to verify the window selected. For the x-axis, due to the specific interest in the wake region for this paper, a sample is taken exclusively in the wake region itself. Furthermore, to eliminate the detrimental effect of the rigid and flexible structure within the final image, the structures have been masked and removed with the main region of interest being that of the flow field itself.

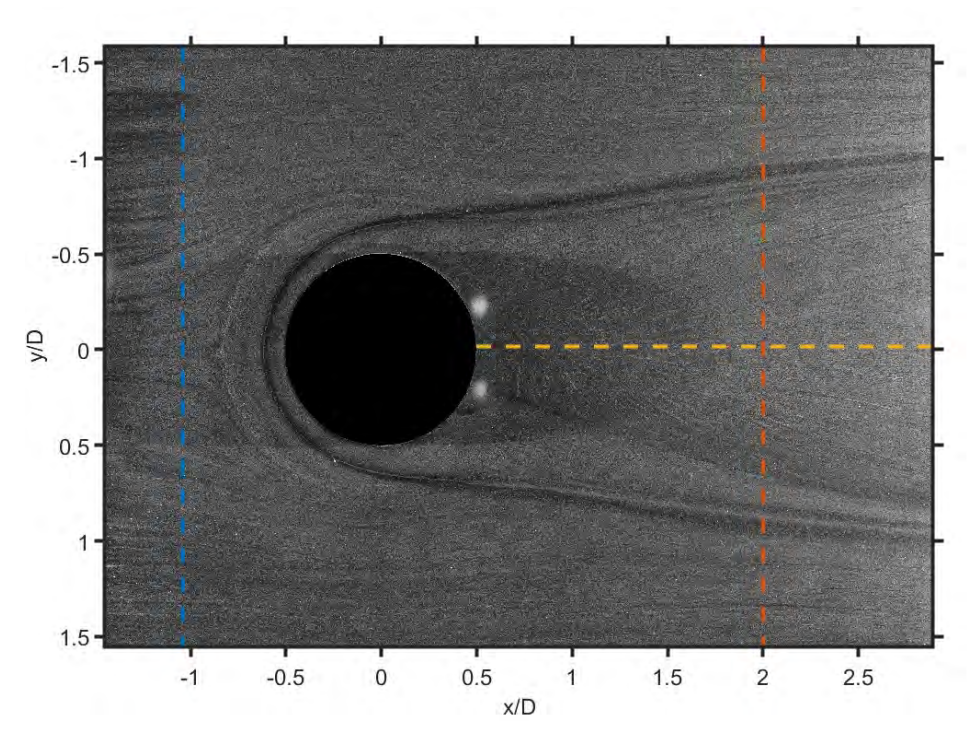


Figure 11 - Gray-scale input image with location data

Once the data samples as shown in figure 11 are extracted, this is then passed through an autocovariance algorithm to identify the pixel positions within the datasets extracted. The primary purpose of this is the elimination of the higher frequency noise in the image to prevent false detection from the Canny algorithm. The method by which noise is removed is the usage of pixel-windowing within the frequency domain of the original image. The auto-covariance observes the frequency of repeating patterns within the test samples taken. For the purposes of the elimination of the high frequency results, they have been assumed to be concentrated in the region of spatial lag = 0 pixels. To interpret this, regions at which spatial lag \approx 0 pixels are associated with noise in the image, as the frequency of visible streamlines is lower than the values surrounding this region. This region contains the largest concentration of image noise. Thus, the point selected to create a FFT window was selected as the region in both x and y at which the normalised magnitude of the auto-covariance passes 0. This

consistently shows the elimination of the higher frequency components. This cutoff point is selected separately for both the x and the y components, with the average taken between the upstream and the downstream dataset. Thus, figure 12 presents an example of the auto-covariance data extracted from figure 11. Furthermore, the subsequently created window within the frequency domain is presented within figure 13, where all pixels external to the window have been set to 0.

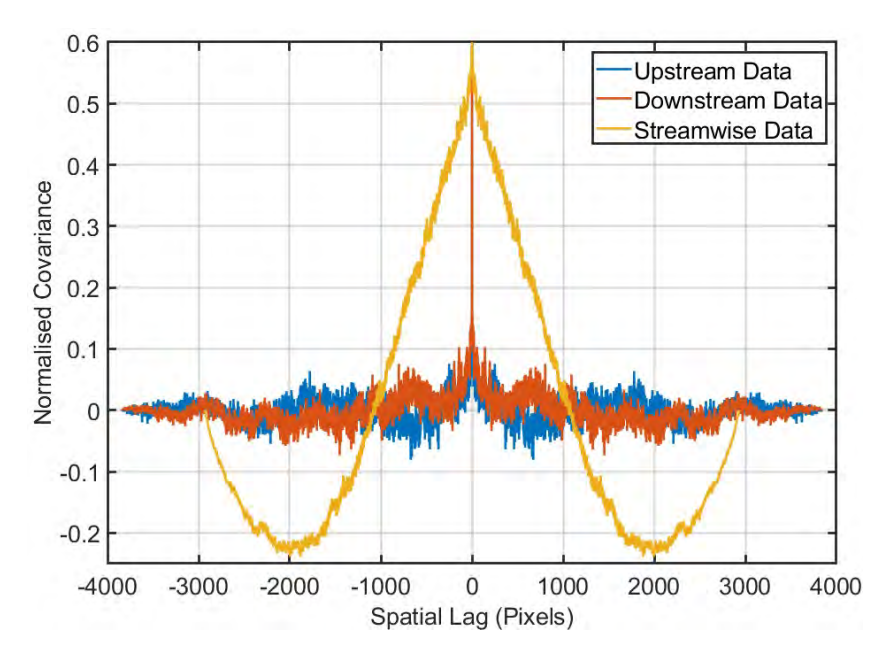


Figure 12 – Normalised co-variance of the streamwise and spanwise data

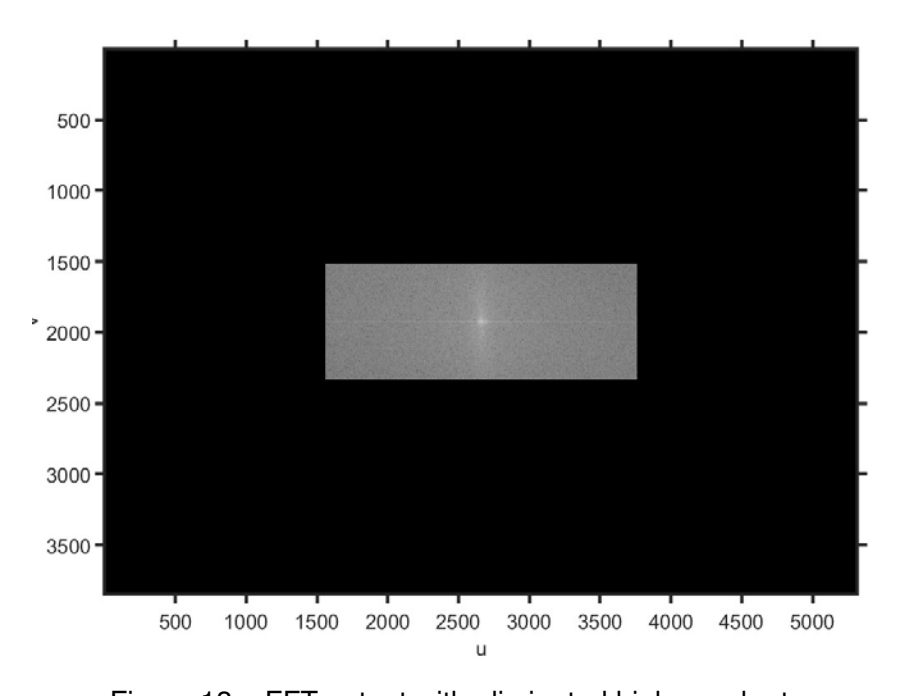


Figure 13 – FFT output with eliminated higher order terms

Following the windowing process, the final processing operation is to complete the inverse FFT operation allowing for the reproduction of the averaged image for each velocity case, for both the rigid and flexible hemispheres. This can be observed in figure 14. Comparative to the raw image shown in figure 11 the higher frequency noise has been reduced, which can be directly observed when comparing these two figures. This allows for the enhancement of regions with large variations in brightness levels, such as regions of reduced or concentrated particle deposition. As seen in figure 14 this results in greater clarity and visibility of bulk flow features such as the edge of the wake region, observed travelling downstream. One negative effect of this method is the elimination of some intri-

cate details within the flow itself, when observing regions with closely placed streamlines, the results can appear to blur due to brightness averaging per pixel. When observing figure 14 the key aspect that can be observed is the clear delineation of the shed vortex structure bounding the wake region. The comparative darkness of this region can be linked to the vortex structure forcing the oil mixture to push further into the freestream or further into the out of plane axis. For other velocity cases, such as shown in figure 7, this region contains a higher concentration of particles. This indicates there may be a degree of 3-dimensional flow interaction not captured within this analysis process. Thus, for the analysis in the paper, this aspect of the flow will be observed, particularly the growth and the asymmetry of the region.

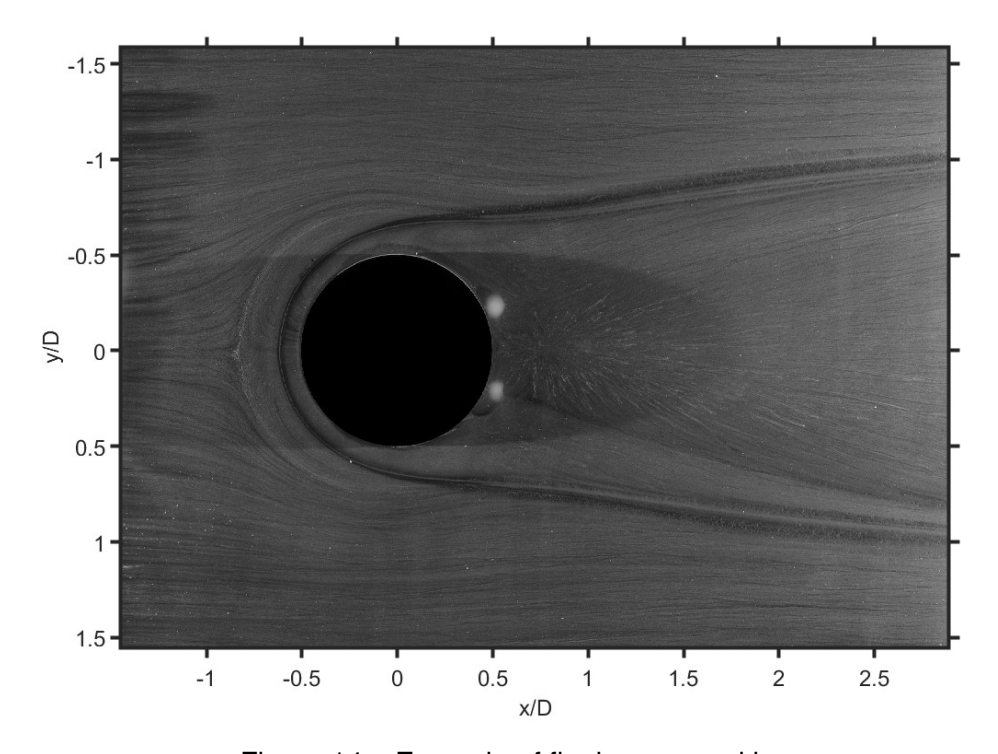


Figure 14 – Example of final processed image

The processed image is then utilised within the Canny algorithm to detect the edges of the features within the final image (figure 14). When implementing the Canny algorithm for the purposes of the final data extraction, the input parameters alter the result. The two considerations made are the threshold for the features of interest and the selected value of σ , where σ is the standard deviation utilised within the Gaussian filter utilised within the Canny algorithm. For the purposes of this paper, the threshold limits are set to enable the extraction of the edge features of concern. This being the wake width dimension. Due to minor variation in light levels and contrast between test cases, the input images of the Canny algorithm were adjusted as needed to extract the relevant information. Figure 15 shows the effect of a lower range σ value. Critically the wake formation can clearly be observed, however due to the minimal use of the Gaussian filter, the small-scale features appear within the image clearly. Which indicates that the processing has resulting in the desired effect, allowing for the processing method to be effectively utilised for future analysis of smaller flow features in specific regions of interest within the complete flow field. For analysis of small scale, a low Gaussian filter would be required with substantial resolution provided as seen in figure 15. For this paper, the primary value of concern is the increase in the wake width travelling downstream, figure 16 shows a large degree of smoothing occurring within the Canny algorithm. This eliminates most of the small scale flow features. This shows the boundary of the two flow regions, the freestream flow and the wake region. Within these two regions, small flow features contain a minimal intensity gradient change, as the oil distribution deposits particles as expected. Due to this, the pixel to pixel intensity gradients do not change with sufficient magnitude once the Gaussian filter is applied to the Canny algorithm to effectively detect an edge.

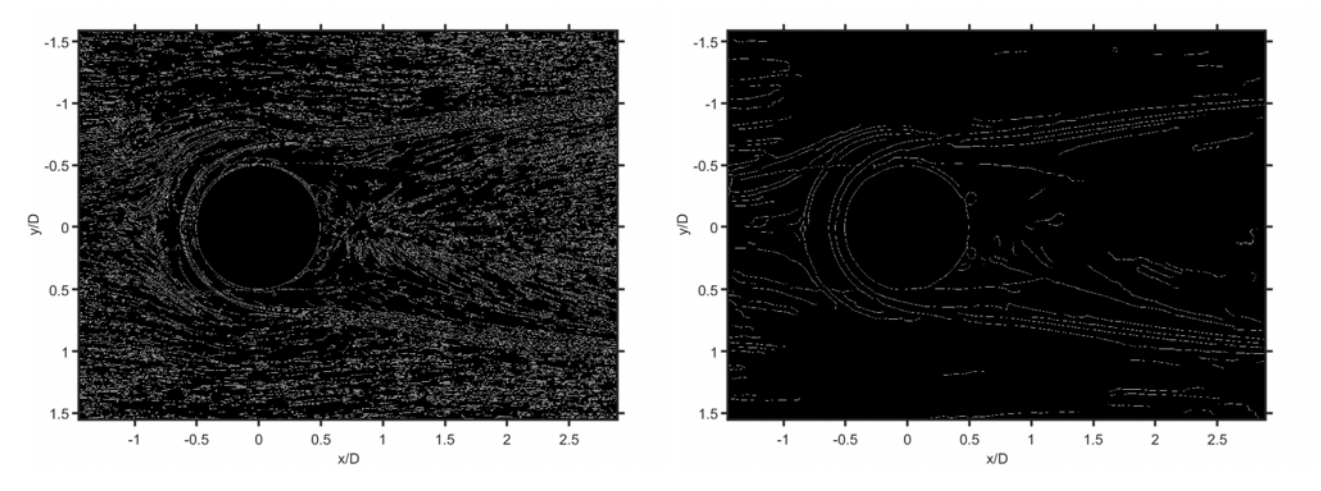


Figure 15 – Example of Edge Detection (Canny) using the Rigid Model at 40m/s with $\sigma = 5$

Figure 16 – Example of Edge Detection (Canny) using the Rigid Model at 40m/s with $\sigma = 20$

For the purposes of this paper, the higher level of smoothing ($\sigma=20$) is utilised to extract only the regions at which substantial change occurs, which from observation is seen to be at the edge of the wake region itself. When compared with a range of σ values, $\sigma=20$ appeared to show consistent edge detection for the features of interest with minimal noise. To track the wake growth along the streamwise dimension, a spanwise sample is taken at fixed intervals and used to compare the result between flow speed, and model type. Figure 17 presents an example of a spanwise sample taken at 2D downstream from the rigid hemisphere. When compared to the direct sampling of the filtered input image, the exact location is easier to determine utilising the edge detection method, the large central gap showing the central region of the wake. However, to process this, the elimination of some minor elements must be considered. Through observation, the lower edge of the wake (relative to figure 16) occurs at y/D>0.5. However, the edge detection has identified other false edges in the flow. Hence, comparison must be made to verify that false positives have not caused errors in the final solution. Within the detected edges a clear asymmetry can be observed between the starboard and port side of the wake, which will be further analysed by this technique.

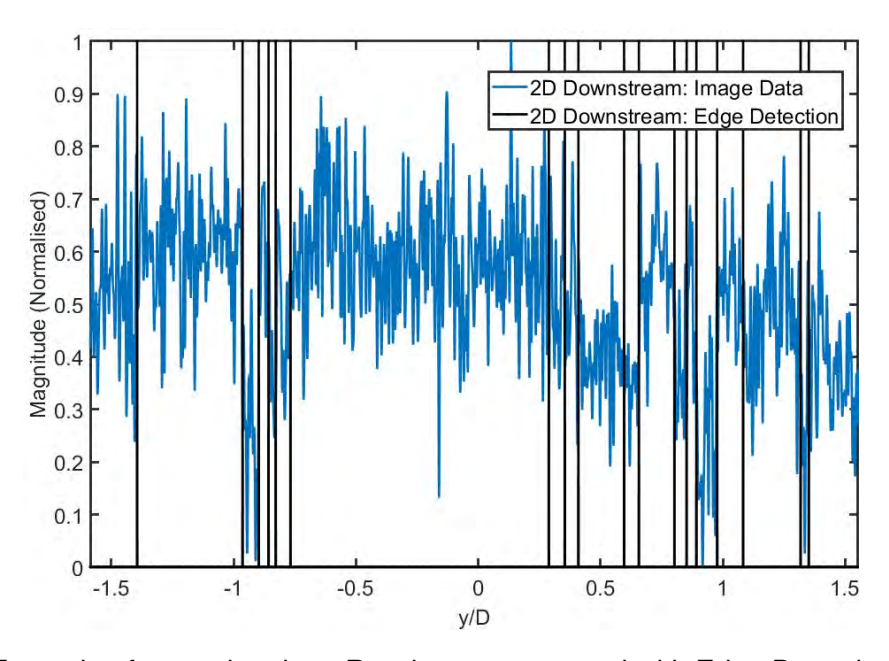


Figure 17 – Example of spanwise data, Raw image compared with Edge Detection with $\sigma = 20$

3.3 Final Result

To obtain final comparison of results around the models, the edge detection method is utilised to observe the time-averaged wake dimensional changes. For this analysis, the large-scale flow characteristics are observed, specifically the size of the wake region itself. Bounded by the region of high shear and the asymmetry of the wake. The wake region is defined as the inner distance between the regions of high shear, as described in section 3.1. The results of the flexible model and rigid model are shown in figure 18 and figure 19 respectively. Where the distances taken originate at the trailing edge of the hemisphere to the furthest downstream position within the region of interest. The key aspect that is common between both models is the increase in wake size as samples are taken downstream. This is expected behaviour for flow around a hemisphere, as described within section 1.1, however an unexpected observation from the results is the minimal change in dimension between velocity cases. As the velocity increases, the general trend for both models shows an increase in wake size, however this is not shown as consistent. This could be linked to one of two primary reasons. The first being false detections within the edge detection algorithm. Though an aggressive Gaussian smoothing value is chosen, this may still result in smaller feature detection, thus causing an apparent smaller wake. The second reason being linked to the flow features downstream, such as flow instabilities masking the exact boundary at which the wake transitions into the freestream. This is more evident at lower velocities. At lower flow velocities the rate of wake growth, relative to the start position is increased, with the rate being larger for the flexible model, as compared to the rigid. When observing the wake size at 15m/s, the flexible hemisphere shows a wake size increase of 68% at 2D compared to 0.5D, the rigid model at 15m/s only shows an increase of 25%. As the flow velocity increases the trends is maintained, whereby the downstream region indicates a larger wake size with a lower change between the first and last data point, in essence a lower gradient. At 40m/s the increase in size for the flexible model decreases to 25% growth whereas the rigid model wake size growth is 26%. This indicates that the rigid model shows a consistent gradient of wake growth with changing velocities, with the absolute values being the primary variation. Whereas the flexible model, at lower speeds show smaller wake sizes near the structure itself. However there is a substantial increase in downstream wake size. As the results indicate, no clear trend dependent on velocity is observable, with the only consistency being attributed to the relative wake size growth percentage.

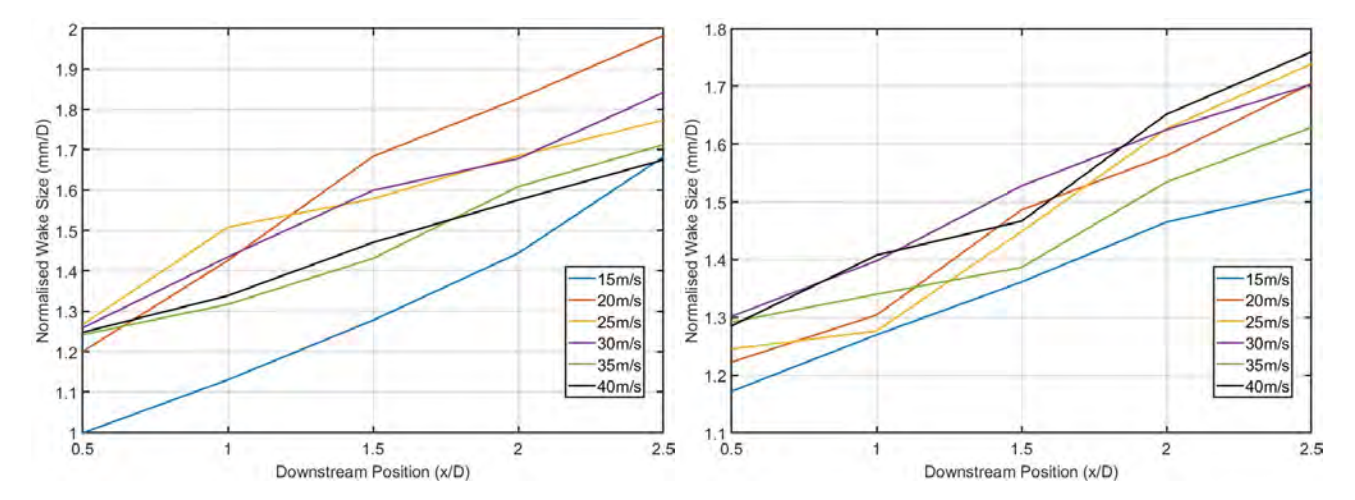


Figure 18 – Change in wake size with velocity of the Flexible Model the Rigid Model

In addition to viewing the growth in the wake, a key indication of fluid structure interaction is the average spanwise flow asymmetry. Figure 20 and figure 21 show that there is a large degree of asymmetry in the wake region. The flexible model, shows a larger peak asymmetry from the centreline, with velocities greater than 20m/s causing the wake structure to trend towards the port size of the hemisphere structure. Initially a spike to the starboard side is visible at 15m/s and 20m/s however subsequently as the flow speed increases to 40m/s the asymmetry of the wake increases,

peaking at a y/D = 0.4731. This increase indicates that as the speed of flow increases, the fluid structure interaction caused by the deformation of the flexible hemisphere causes an overall time averaged downstream flow effect, shifting the flow towards the port direction of the hemisphere. This is somewhat visible when observing the flow around the flexible model in figure 8 which indicates a pattern of asymmetry in the wake. Overall the magnitude of this asymmetry is larger for the flexible model as compared to the rigid model results shown in figure 21 which shows comparatively minimal variation. This is expected, as the flow around a typical hemisphere when time averaged should show a relatively symmetrical downstream flow pattern, as there are no other effects causing flow variation. However, in the near wake, a large change is observable at lower velocities. At 15m/s there is indicated shift of y/D = 0.119 to the port side which decreases with speed and eventually flipping to a starboard trending wake at 40m/s, shifting to y/D = -0.0186. This can be linked to general turbulence or flow instability at the lower tunnel operating speed. However, without further investigation, this can not be concluded definitively. As previously mentioned, due to the nature of implementation of the edge detection algorithm, false edge detections are possible, indicating that some asymmetry of the rigid flow could be attributed to this effect. However, as the magnitudes remain comparably low, this may indicate confidence in the detected edges as real boundaries of the wake region.

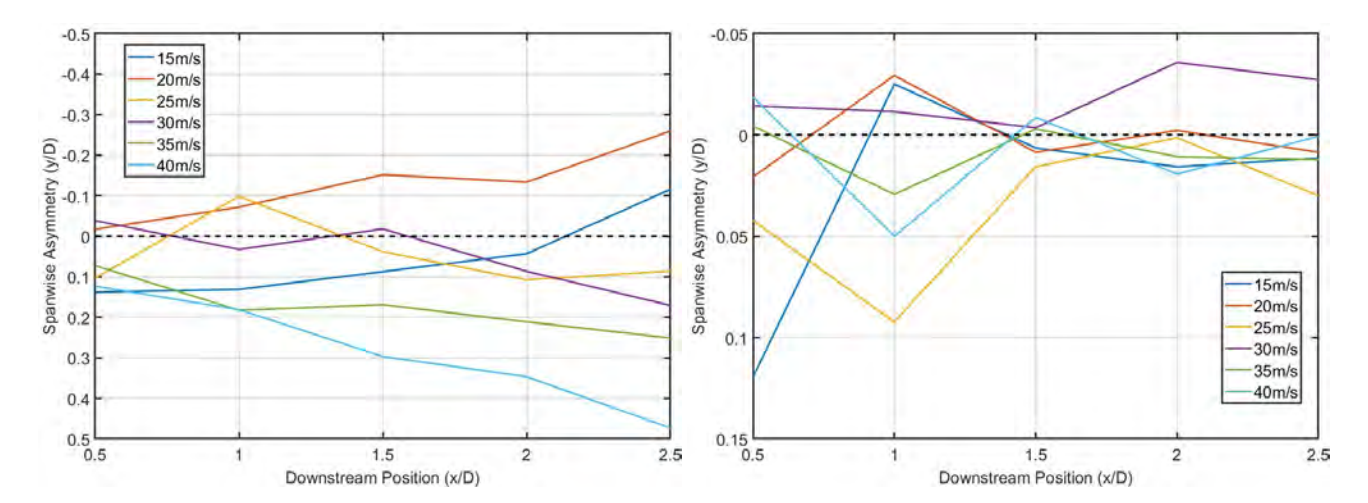


Figure 20 – Span-wise wake asymmetry of the Flexible Model

Figure 21 – Span-wise wake asymmetry of the Rigid Model

4. Conclusions

When analysing the flow visualisation, the raw images contain a high level of noise in the image, caused by the fluctuations in light levels from the test setup. To alleviate this, an average image was employed to eliminate the higher frequency noise. This produced an image for Canny edge detection. The Canny algorithm has extracted both small scale and large-scale flow features. The key parameter which allowed this is the σ term, which denotes the effect of the Gaussian smoothing within the Canny algorithm. The analysis has shown that bulk features are easily resolved using edge detection, particularly the locations at which high shear or flow separation occurs. These regions show a substantial change in the image intensity gradient, allowing extraction and quantification of edges.

For this analysis, an aggressive Gaussian filter was selected to allow for the extraction of the key parameters. For this paper, this includes the wake growth downstream and the asymmetry of the wake, dependent on incoming flow velocity. This was conducted with both a flexible structure and a rigid structure to observe the variation caused by the fluid-structure interaction. The results indicate that the wake growth for both structures did not show a clear trend with varying velocities. However, this could be attributed to the effect of false edge detection during the Canny algorithm implementation. The flexible model is shown to present a consistently larger rate of wake growth compared to the rigid model, with the average gradient at 15m/s calculated to be 0.34 and 0.17 for the flexible model and rigid model respectively. This changes at 40m/s to 0.21 and 0.23 for the flexible model and rigid

model. The larger absolute wake width occurs at 20m/s for the flexible model at a position 2.5D downstream, showing a wake size of y/D = 1.98.

The flexible model is also consistently shown to present larger absolute wake growth compared to that of the rigid. Furthermore, the flexible model has larger levels of asymmetry in the wake, which increases with speed from y/D=-0.116 (port) at 15m/s to y/D=0.473 (port) at 40m/s. This is not present in the rigid model, which indicates lower wake asymmetry the further downstream measurements are taken. Here, the largest region of asymmetry is located immediately aft of the structure at 0.5 with a variation from y/D=0.119 (port) at 15m/s to y/D=-0.019 (starboard) at 40m/s.

Overall, the results have shown that the usage of Canny edge detection is effective for the application of quantifying data, from a qualitative technique such as oil visualisation. With use of flow visualisation techniques with larger image intensity gradients such as Schlieren photography, this method could be used effectively. Furthermore, this method has allowed for the characterisation of the time averaged downstream behaviour of a flexible structure as compared with a rigid structure, showing the variation due to fluid structure interaction.

5. Contact Author Email Address

mailto: nishanth.menakath@sydney.edu.au

6. Copyright Statement

The authors confirm that they, and/or their company or organisation, hold copyright on all of the original material included in this paper. The authors also confirm that they have obtained permission, from the copyright holder of any third party material included in this paper, to publish it as part of their paper. The authors confirm that they give permission, or have obtained permission from the copyright holder of this paper, for the publication and distribution of this paper as part of the ICAS proceedings or as individual off-prints from the proceedings.

References

- [1] F.K. Lu. Surface oil flow visualization: Still useful after all these years. *The European Physical Journal Special Topics*, 182(1):51–63, April 2010.
- [2] Mehti Koklu. Effects of sweeping jet actuator parameters on flow separation control. *AIAA Journal*, 56(1):100–110, January 2018.
- [3] E. Savory and N. Toy. The flow regime in the turbulent near wake of a hemisphere. *Experiments in Fluids*, 4(4):181–188, 1986.
- [4] J. M. McCarthy, M. Giacobello, and S. Lam. Wavelet coherence of surface pressure fluctuations due to von kármán vortex shedding near a hemispherical protuberance. *Experiments in Fluids*, 60(1), November 2018.
- [5] Michael Manhart. Vortex shedding from a hemisphere in a turbulent boundary layer. *Theoretical and Computational Fluid Dynamics*, 12(1):1–28, July 1998.
- [6] Nishanth Menakath, Gareth A. Vio, Nicholas J. Lawson, and Nicholas F. Giannelis. *Experimental investigation of pressure fluctuations around protuberances of varying shapes*. January 2023.
- [7] Ian A. Carr and Michael W. Plesniak. Three-dimensional flow separation over a surface-mounted hemisphere in pulsatile flow. *Experiments in Fluids*, 57(1), December 2015.
- [8] J.N. Wood, M. Breuer, and G. De Nayer. Experimental studies on the instantaneous fluid–structure interaction of an air-inflated flexible membrane in turbulent flow. *Journal of Fluids and Structures*, 80:405–440, July 2018.
- [9] R. L. Maltby. Flow visualization in wind tunnels using indicators. 1962.
- [10] J. C. R. Hunt, C. J. Abell, J. A. Peterka, and H. Woo. Kinematical studies of the flows around free or surface-mounted obstacles; applying topology to flow visualization. *Journal of Fluid Mechanics*, 86(1):179–200, May 1978.
- [11] W. Merzkirch, K. Gersten, North Atlantic Treaty Organization. Advisory Group for Aerospace Research, and Development. Fluid Dynamics Panel. *Techniques of Flow Visualization*. Number no. 302 in AGAR-Dograph. AGARD, 1987.
- [12] Yong Cao and Tetsuro Tamura. Large-eddy simulation study of reynolds number effects on the flow around a wall-mounted hemisphere in a boundary layer. *Physics of Fluids*, 32(2), February 2020.

Surface visualisation of time averaged flow behaviour around rigid and flexible structures utilising UV sensitive

- [13] M Tobak and D J Peake. Topology of three-dimensional separated flows. *Annual Review of Fluid Mechanics*, 14(1):61–85, January 1982.
- [14] Daniel Simmons, Flint O. Thomas, and Thomas C. Corke. Smooth body flow separation experiments and their surface flow topology characterization. June 2019.
- [15] John Canny. A computational approach to edge detection. *IEEE Transactions on Pattern Analysis and Machine Intelligence*, PAMI-8(6):679–698, November 1986.
- [16] Irina Znamenskaya, Igor Doroshchenko, and Daria Tatarenkova. Edge detection and machine learning approach to identify flow structures on schlieren and shadowgraph images. *Proceedings of the 30th International Conference on Computer Graphics and Machine Vision (GraphiCon 2020). Part 2*, pages paper15–1, 12 2020.
- [17] Takeshi R. Fujimoto, Taro Kawasaki, and Keiichi Kitamura. Canny-edge-detection/rankine-hugoniot-conditions unified shock sensor for inviscid and viscous flows. *Journal of Computational Physics*, 396:264–279, November 2019.
- [18] Tarek Abdelsalam, Richard Williams, and G. Ingram. Exploiting modern image processing in surface flow visualisation. 01 2017.
- [19] Fude Guo, Yahui Yang, Bin Chen, and Liejin Guo. A novel multi-scale edge detection technique based on wavelet analysis with application in multiphase flows. *Powder Technology*, 202(1–3):171–177, August 2010.